Sensors and Materials, Vol. 36, No. 10 (2024) 4205–4220
MYU Tokyo

S & M 3795

Dynamic Stability Analysis of Magnetically Levitated Rotor in a Nutation Blood Pump

Gang Chen and Kun-Chieh Wang*

School of Mechanical and Electric Engineering, Sanming University, Sanming, Fujian 365004, China

(Received April 30, 2024; accepted September 17, 2024)

Keywords: magnetic levitation, blood pump rotor, levitation stability, nutation blood pump

Improving the performance of nutation blood pumps has long been a focus of medical research. In this study, we introduce the finite element method combined with sensor-based experimental measurements to explore the factors affecting the stability of the levitated magnetic rotor in the blood pump. Initially, we derived Euler angle and motion state equations to describe the motion of the magnetically levitated rotor inside the blood pump. Subsequently, employing the finite element method, we analyzed various factors impacting the dynamic levitation stability of the rotor. Our results indicate that the size of the permanent magnet in the rotor bearing, the nutation angle, and the levitation gap are critical factors affecting the rotor's levitation stability. We discuss these crucial parameters in detail, highlighting their correlation with the levitation stability of the rotor. Furthermore, comparing our theoretically obtained magnetic forces with experimental results, we found the maximum difference to be within 8%. Overall, this study provides valuable insights to enhance the functionality of blood pumps and understand the key parameters affecting their design.

1. Introduction

The dynamic stability of the levitated rotor directly impacts the performance and reliability of magnetic levitation blood pumps. These pumps typically employ an axially passive permanent magnetic bearing as a key element in their internal motion mechanism. The stability of this passive permanent magnetic bearing within the blood pump cavity is the primary factor affecting the pump's performance. Ensuring a stable levitation of the passive permanent magnetic bearing requires the internal rotor to achieve stability in both radial and axial directions.

Chen *et al.* studied the levitation stability of passive magnetic bearings in blood pump rotors.[1] They discovered that the rotor stability increased with rotor speed. At 2300 rpm, the maximum disturbance of the levitation gap was only 0.2 mm.[1] Chen *et al.* investigated the design of a novel passive magnetic levitation rotor blood pump for ventricular assist devices. Through hydraulic experiments, they determined that the pump could achieve pressures of 60–140 mmHg at rotational speeds of 600–1600 rpm, flow rates of 0.4–6.7 L/min, and a

*Corresponding author: e-mail: m18316252102@126.com
https://doi.org/10.18494/SAM5109

ISSN 0914-4935

normalized hemolytic index (NIH) for the nutrient pump of 0.0043 ± 0.0008 g/100 L. *In vitro* experiments demonstrated that the magnetically levitated ventricular assist commutated blood pump exhibited good levitation stability and feasibility for animal testing.(2) Wang *et al.* developed a novel bearingless axial blood pump utilizing magnetic double suspension.(3) They established an external circulation experimental system to test this pump, conducting experiments to measure the axial and radial displacements of the rotor under various operating conditions using Hall effect sensors and a laser vibrometer.(3) Shen *et al.* devised an innovative magnetic levitation bearing, combining a single-winding bearingless motor with a permanent magnet bearing.(4) They used the solution of the Reynolds equation and stiffness analysis to determine the optimal structural parameters for this bearing, exploring various factors through computational fluid dynamics (CFD). Their vibration experiments demonstrated that the rotor of the blood pump equipped with this magnetic levitation bearing exhibited excellent levitation stability, with the maximum deflection under external fluid impact not exceeding 2 μm.(4) Chen *et al.* created an innovative magnetically levitated (maglev) nutation blood pump designed for low speed and small volume flow rate, effectively eliminating friction damage to blood cells.(5) *In vitro* experiments demonstrated that the pump can sustain an output of more than 5 L/min under a pressure load of 100 mmHg, with the pump's output flow remaining stable under various pressures. The NIH of this nutation pump was measured at 0.0039 ± 0.0006 g/100 L.(5) Shida *et al.* studied the impact of gravity on flow estimation in centrifugal blood pumps with suspended impellers.(6) They analyzed the effect of gravity on flow estimation methods and proposed a compensation technique.(6) Kosaka *et al.* introduced an analytical approach to enhance hemolysis performance in a hydrodynamically levitated centrifugal blood pump by optimizing the shroud size.(7) They showed that numerical analysis was effective in determining the optimal shroud size and proposed a specific blood pump model with an optimal shroud size to minimize hemolysis.(7) Luo *et al.* investigated the performance of passive magnetic bearings in a pediatric left ventricular assist device (LVAD) magnetic levitation blood pump system.(8) They developed a pediatric LVAD utilizing noncontact magnetic bearings, which include passive and active magnetic bearings, to minimize blood trauma and extend device lifespan.(8) Miyamoto *et al.* explored the effect of nutation orientation on blood pump performance, specifically examining pulse pressure and regurgitant flow when the pump is halted.(9) Their findings indicate that nutation orientation has a minimal effect on pump performance, showing no impact on pulse pressure or regurgitant flow during pump stoppage.(9) Yang *et al.* employed CFD to investigate the flow channel optimization and performance prediction of a cone-shaped axial magnetic levitation blood pump.(10) Their study focused on using magnetic levitation support to minimize blood damage and extend the pump's lifespan.(10) Li *et al.* conducted a thorough comparison of the *in vitro* blood compatibilities of extracorporeal centrifugal blood pumps.(11) They emphasized the importance of *in vitro* blood compatibility testing for assessing the side effects of transit blood pumps, providing a necessary reference for evaluating blood-pump-induced blood injury before clinical trials.(11) Wu reviewed the current state of high-fidelity blood flow and blood damage simulation methods, including CFD, employed in the development and evaluation of rotary blood pumps.(12) Shida *et al.* presented a research methodology to determine the time resolution and accuracy of the dynamic movement of a levitated impeller.(13) Their investigation

demonstrated that the target levitated impeller blood pump is suitable for use as a ventricular assist device, operating at speeds exceeding 1800 rpm above the resonant frequency. The rotor's dynamic forces (ranging from 0.03 to 0.14 N) on the impeller suppressed its rotational movement, indicating a stable dynamic motion.[13] Ranganath *et al.* conducted a review focusing on the theoretical design and operational principles of mechanical bearings in blood pumps.[14] They discussed the challenge of thrombosis within these mechanical bearings, highlighting it as an inherent design parameter issue beyond the control of clinicians.[14] Fox *et al.* designed a centrifugal blood pump by employing CFD to analyze the blood flow within the pump.[15] They conducted transient CFD analysis, including quasi-steady and transient rotating sliding interfaces, to assess the pump's dynamic performance under various conditions.[15] Li *et al.* investigated the impact of rotor design configuration on the hemodynamic characteristics, blood compatibility, and dynamic balance of a blood pump.[16] They utilized CFD to analyze how rotor types (closed and semi-open impellers), gap height, and back blades affect the pump's performance.[16] Several other studies have focused on the local performance of centrifugal maglev blood pumps and the factors that affect them.[17–21]

From the previous literature review, it is evident that most studies have focused on investigating the factors affecting blood pump performance or on designing blood pumps with optimal functionality. These include studies on the optimal design of rotor components such as blades, utilizing methods such as CFD or experiments. However, there are few comprehensive discussions on the factors affecting the performance of pulsatile blood pump bearings.

Therefore, we intend to introduce the finite element method combined with sensor-based experimental measurements to examine three key factors affecting the stability of pulsatile blood pump bearings: the size of the permanent magnet, the nutation angle, and the levitation air gap. The aim is to explore the effects of these factors on the levitation stability of the blood pump rotor.

2. Analysis of Motion State of Magnetically Levitated Rotors

2.1 Euler angle equation

The magnetically levitated blood pump rotor consists of an upper and lower ball pair and a nutation disc fixed together. Permanent magnets are embedded in the upper and lower ball pairs, aligned with magnetic poles in the upper and lower covers, generating repulsive forces to suspend the rotor. Seven axially magnetized fan-shaped permanent magnets are arranged at the rotor's edge, all with the same magnetic pole direction. Two driving permanent magnets, arranged symmetrically with opposite magnetic poles, attract magnets on one side of the nutation disc and repel those on the other side, causing the nutation disc to tilt. This disc maintains linear contact with the inner conical surfaces of the upper and lower covers. As the driving magnets rotate, the nutation disc undergoes directed nutation oscillation, facilitating directed blood flow inside the pump. The pump and rotor structure are depicted in Fig. 1.

To describe the motion of the blood pump rotor, we established two sets of coordinate systems: a rigid rotor kinematic coordinate system and a fixed coordinate system, as shown in

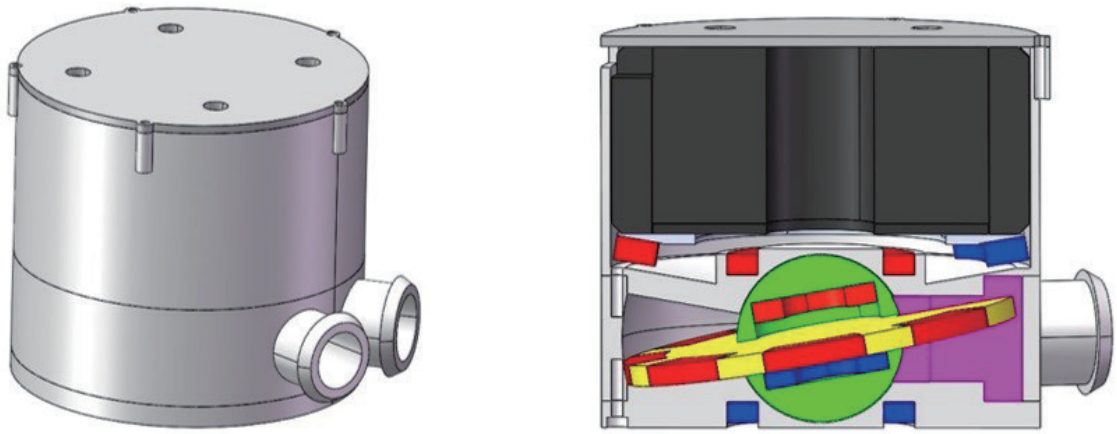

Fig. 1. (Color online) Layout of magnetic nutation blood pump and its inner rotor.

Fig. 2. The blood pump rotor can be viewed as a rotating rigid body symmetrical to its rotation axis. Its kinematic coordinate system is firmly attached to the rotor, with the rotor's main axis known as the inertia main or polar axis. The axis perpendicular to the symmetry axis is called the equatorial axis. The moment of inertia around the rotor axis is termed the polar moment of inertia, while taht around the equatorial axis as the reference axis is called the equatorial moment of inertia.

Generally, any rotational motion of a rigid body in an inertial coordinate system must follow the familiar theorem of angular momentum conservation. However, in the case of the rigid-body rotor in this study, its rotational inertia and inertial product with respect to the inertial coordinate system are time-varying. This necessitates real-time coordinate transformations, making the application of the theorem of angular momentum conservation cumbersome in computation.

Instead, Euler's kinetic equations utilize a dynamic coordinate system, simplifying the analysis and calculation. By using this dynamic coordinate system as the reference, we can describe the angular momentum conservation theorem applicable to the rotational motion of the blood pump rotor as follows.

For the motion of the blood pump rotor, we assumed that O is the origin of the dynamic coordinate system, and $\boldsymbol{i}$, $\boldsymbol{j}$, and $\boldsymbol{k}$ are the unit vectors in the x-, y-, and z-directions of the Cartesian coordinate system. The angular momentum of the blood pump rotor can be expressed in the dynamic coordinate system as

$$\boldsymbol{H} = H_x\boldsymbol{i} + H_y\boldsymbol{j} + H_z\boldsymbol{k}\,. \tag{1}$$

Then, the relationship between the applied moment and the angular momentum can be expressed as

$$\begin{aligned}\boldsymbol{M} &= \frac{\mathrm{d}\boldsymbol{H}}{\mathrm{d}t} = \frac{\mathrm{d}}{\mathrm{d}t}(H_x\boldsymbol{i} + H_y\boldsymbol{j} + H_z\boldsymbol{k}) \\ &= \frac{\mathrm{d}H_x}{\mathrm{d}t}\boldsymbol{i} + \frac{\mathrm{d}H_y}{\mathrm{d}t}\boldsymbol{j} + \frac{\mathrm{d}H_z}{\mathrm{d}t}\boldsymbol{k} + H_x\frac{\mathrm{d}\boldsymbol{i}}{\mathrm{d}t} + H_y\frac{\mathrm{d}\boldsymbol{j}}{\mathrm{d}t} + H_z\frac{\mathrm{d}\boldsymbol{k}}{\mathrm{d}t}\,.\end{aligned} \tag{2}$$

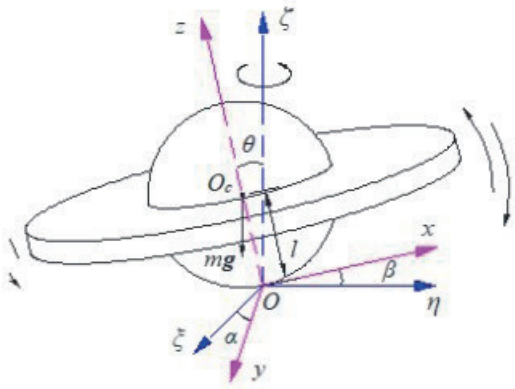

Fig. 2. (Color online) Coordinate systems of blood pump rotor.

We assumed that the angular velocity of the dynamic coordinate system *O*-*xyz* with respect to the inertia coordinate system *O*-$\xi\eta\zeta$ is ω_1; then, d$\boldsymbol{i}$/dt, d$\boldsymbol{j}$/dt, and d$\boldsymbol{k}$/dt in Eq. (2) can be expressed as

$$\begin{cases} \dfrac{\mathrm{d}\boldsymbol{i}}{\mathrm{d}t} = \omega_1 \times \boldsymbol{i} \\ \dfrac{\mathrm{d}\boldsymbol{j}}{\mathrm{d}t} = \omega_1 \times \boldsymbol{j} \\ \dfrac{\mathrm{d}\boldsymbol{k}}{\mathrm{d}t} = \omega_1 \times \boldsymbol{k} \end{cases}. \tag{3}$$

Substituting Eq. (3) to Eq. (2), we have

$$\boldsymbol{M} = \frac{\mathrm{d}\boldsymbol{H}}{\mathrm{d}t} + \omega_1 \times \boldsymbol{H}\,. \tag{4}$$

Equation (4) demonstrates that, for the blood pump rotor subjected to an external moment, the rate of change in angular momentum expressed in the inertial coordinate system can be separated into two components. One component represents the rate of change in angular momentum in the dynamic coordinate system, whereas the other component represents the rate of change in angular momentum generated by the angular velocity of the dynamic coordinate system relative to the inertial coordinate system. Equation (4) of the external moment expressed in the dynamic coordinate system, when projected onto the right-angle coordinate system, can be expressed as

$$\frac{\mathrm{d}H_x}{\mathrm{d}t}\boldsymbol{i} + \frac{\mathrm{d}H_y}{\mathrm{d}t}\boldsymbol{j} + \frac{\mathrm{d}H_z}{\mathrm{d}t}\boldsymbol{k} + \begin{vmatrix} \boldsymbol{i} & \boldsymbol{j} & \boldsymbol{k} \\ \omega_x & \omega_y & \omega_z \\ H_x & H_y & H_z \end{vmatrix} = M_x\boldsymbol{i} + M_y\boldsymbol{j} + M_z\boldsymbol{k}\,. \tag{5}$$

Equation (5) can be written in the form of a system of scalar equations, as follows.

$$\dot{H}_x + \omega_y H_z - \omega_z H_y = M_x ,$$

$$\dot{H}_y + \omega_z H_x - \omega_x H_z = M_y , \tag{6}$$

and

$$\dot{H}_z + \omega_x H_y - \omega_y H_x = M_z .$$

The set of scalar Eq. (6) is the kinetic equation of the fixed point motion of the blood pump rotor, also known as Euler's equation. We assumed that the rotor of the blood pump, relative to the inertial coordinate system, rotates around its central axis $O\eta$ with an angle, angular velocity, and angular acceleration of α, $\dot{\alpha}$, and $\ddot{\alpha}$, respectively. We also assumed that the rotor of the blood pump, relative to the inertial coordinate system, rotates around the axis $O\xi$ with an angle, angular velocity, and angular acceleration of β, $\dot{\beta}$, and $\ddot{\beta}$ respectively. The projections of the angular velocity and angular acceleration of the dynamic coordinate system O-xyz relative to the inertial coordinate system O-$\xi\eta\zeta$ on the x-, y-, and z-axes of the inertial coordinate system are ω_x, ω_y, ω_z and $\dot{\omega}_x$, $\dot{\omega}_y$, $\dot{\omega}_z$, respectively. We further assumed that the applied moments on the blood pump rotor with respect to the central axes $O\eta$ and $O\xi$ are M_x and M_y, respectively. On the basis of the inertia theorem of moments, when the blood pump rotor is rotating, the relationships among the rotational moment of inertia, gyroscopic moment, angular velocity, and angular acceleration can be expressed as

$$M_{Ix} = -I_{xx}\ddot{\alpha} , \tag{7}$$

$$M_{Iy} = -I_{yy}\ddot{\beta} , \tag{8}$$

$$M_{Gx} = -H\dot{\beta} , \tag{9}$$

$$M_{Gy} = H\dot{\alpha} . \tag{10}$$

From the conservation of moment for a blood pump rotor in motion, we obtain the following kinetic equations:

$$M_{Ix} + M_{Gx} + M_x = -I_{xx}\ddot{\alpha} - H\dot{\beta} + M_x = 0 , \tag{11}$$

$$M_{Iy} + M_{Gy} + M_y = -I_{yy}\ddot{\beta} + H\dot{\alpha} + M_y = 0 . \tag{12}$$

2.2 Motion analysis of blood pump rotor

We further characterize the coordinate systems describing the state variables of the blood pump rotor in motion. First, assuming that the rotor of the blood pump rotates around a fixed point O, we can establish an inertial coordinate system O-$\xi\eta\zeta$ and a momentum moment coordinate system O-XYZ on the basis of the origin O, as shown in Fig. 3. The Z axis of the momentum moment coordinate system is consistent with the direction of the momentum moment vector $\boldsymbol{H}$ of the rigid rotor relative to the origin O. Assuming that the original inertial coordinate system O-$\xi\eta\zeta$ rotates around the axis ξ by an angle α, we call this new coordinate system as O-$\xi_1\eta_1\zeta_1$. Then this coordinate system rotates around the axis η_1 by an angle β, and we call the obtained coordinate system as O-XYZ.

The orientation relationship between the momentum moment coordinate system O-XYZ and the inertial coordinate system O-$\xi\eta\zeta$ can be expressed as an orientation cosine matrix:

$$\boldsymbol{C}_{\xi}^{\boldsymbol{X}} = \begin{pmatrix} \cos\beta & 0 & \sin\beta \\ \sin\alpha\sin\beta & \cos\alpha & -\sin\alpha\cos\beta \\ -\cos\alpha\sin\beta & \sin\alpha & \cos\alpha\cos\beta \end{pmatrix}. \tag{13}$$

The momentum moment vector of the blood pump rotor can be expressed as

$$\boldsymbol{H} = H\boldsymbol{Z}^0. \tag{14}$$

As the orientation of the momentum moment $\boldsymbol{H}$ changes, the coordinate system O-XYZ will change accordingly and its rotational velocity is denoted as ω_H, which can be expressed as

$$\boldsymbol{\omega}_H = \dot{\alpha}\cos\beta\boldsymbol{X}^0 + \dot{\beta}\boldsymbol{Y}^0 + \dot{\alpha}\sin\beta\boldsymbol{Z}^0. \tag{15}$$

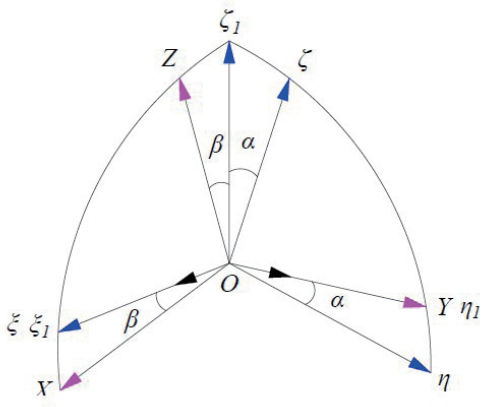

Fig. 3. (Color online) Momentum moment coordinate system and orientation of momentum moment vector.

Assuming that there is a combined moment $\boldsymbol{M}$ with respect to the point O acting on the rotor of the blood pump, its projection in the coordinate system O-XYZ can be expressed as

$$\boldsymbol{M} = M_X \boldsymbol{X}^0 + M_Y \boldsymbol{Y}^0 + M_Z \boldsymbol{Z}^0 . \tag{16}$$

In accordance with the general relationship between the moment and the angular momentum, using Eqs. (14)–(16), we obtain

$$H\dot{\beta} = M_X , \tag{17}$$

$$H\dot{\alpha}\cos\beta = -M_Y , \tag{18}$$

and

$$\dot{H} = M_Z . \tag{19}$$

To describe the motion of the blood pump rotor relative to the momentum moment coordinate system O-XYZ, we use Euler angles ψ, ϑ, and φ to describe the rotor's rotational positions. As shown in Fig. 4, first, the momentum moment coordinate system O-XYZ is rotated about the Z-axis by an angle ψ to obtain a new coordinate system O-$X_1Y_1Z_1$. Then, it is rotated about the X_1-axis by an angle ϑ to obtain another coordinate system fixed on the rotor. Since the dynamic blood pump rotor has no spin, its spin angle φ about the Z-axis is zero.

The transformation cosine matrix from the coordinate system O-xyz to the momentum moment coordinate system O-XYZ can be written as

$$\boldsymbol{C}_{\boldsymbol{X}}^{\boldsymbol{x}} = \begin{pmatrix} \cos\psi & -\cos\vartheta\sin\psi & \sin\vartheta\sin\psi \\ \sin\psi & \cos\vartheta\cos\psi & -\sin\vartheta\cos\psi \\ 0 & \sin\vartheta & \cos\vartheta \end{pmatrix}. \tag{20}$$

Using the transformation Eq. (20), we can transform the momentum vector from the coordinate system O-XYZ to the coordinate axis system O-xyz to obtain

$$\boldsymbol{H} = H(\sin\vartheta\,\boldsymbol{j} + \cos\vartheta\boldsymbol{k}) . \tag{21}$$

Assuming that the relative equatorial and polar moments of inertia of the blood pump rotor with respect to the point are represented by A and B, respectively, its momentum moment vector $\boldsymbol{H}$ can be represented as

$$\boldsymbol{H} = A(\omega_x \boldsymbol{i} + \omega_y \boldsymbol{j}) + B\omega_z \boldsymbol{k} . \tag{22}$$

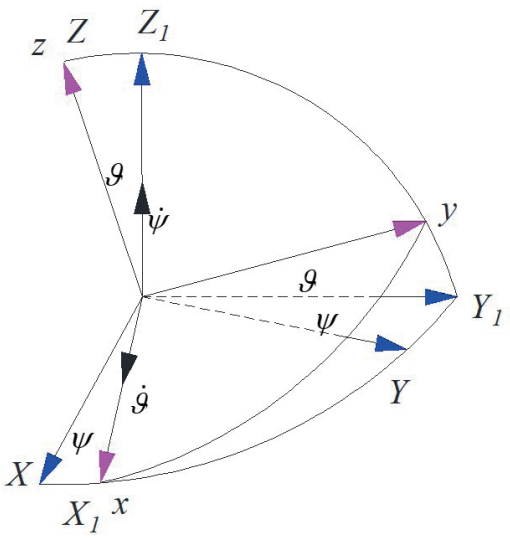

Fig. 4. (Color online) Euler angles of rotor relative to momentum moment coordinate system.

In the above equation, ω_x, ω_y, and ω_z are the projections of the absolute velocity ω of the contact line between the rotor and the upper and lower pump covers onto the x-, y-, and z-axes of the coordinate system O-xyz, respectively, and can be expressed as

$$\begin{cases} \omega_x = \dot{\vartheta} + \dot{\alpha}\cos\beta\cos\psi + \dot{\beta}\sin\psi \\ \omega_y = \dot{\psi}\sin\vartheta + \dot{\alpha}(\sin\beta\sin\vartheta - \cos\beta\cos\vartheta\sin\psi) + \dot{\beta}\cos\vartheta\cos\psi \\ \omega_z = \dot{\psi}\cos\vartheta + \dot{\alpha}(\sin\beta\cos\vartheta + \cos\beta\sin\vartheta\sin\psi) - \dot{\beta}\sin\vartheta\cos\psi \end{cases}. \quad (23)$$

3. Dynamic Stability Analysis of Blood Pump Rotor via CFD

Because the use of the finite element method (FEM) in CFD to analyze rotor motion in blood pumps has been proven to have high calculation accuracy and reliability in previous studies, we are now using this FEM to investigate the dynamic levitation stability of blood pump rotors. First, we establish a structural finite element model of the magnetically levitated nutation blood pump. Then, the motion state equations of the rotor are solved using FEM to understand the 3D motion state of the blood pump rotor. There are two types of material used in the investigated blood pump. First, sintered NdFeB N40 is used for the driving part, which includes the driving permanent magnet and the permanent magnet at the edge of the swing disc. Second, sintered NdFeB N30 is used for the magnetic levitation part, which includes the permanent magnet ring in the pump cover and the swing disc ball pair. The pump body material is selected as stainless steel 316, and other components are considered to be air. Transient solutions for the related physical parameters are obtained by solving the equations mentioned above using FEM.

3.1 Magnetic density distribution around the blood pump rotor

Through FEM calculations, we obtain the magnetic flux density around the blood pump rotor. The 3D distribution of the magnetic density vector and its projection onto the *O-yz* plane around the pump rotor, which significantly affect the levitation stability of the blood pump, are schematically shown in Figs. 5 and 6, respectively. We found that the magnetic flux near the edge of the rotor is significantly different from elsewhere, and the magnetic field variation here has a significant impact on the stability of the rotor levitation.

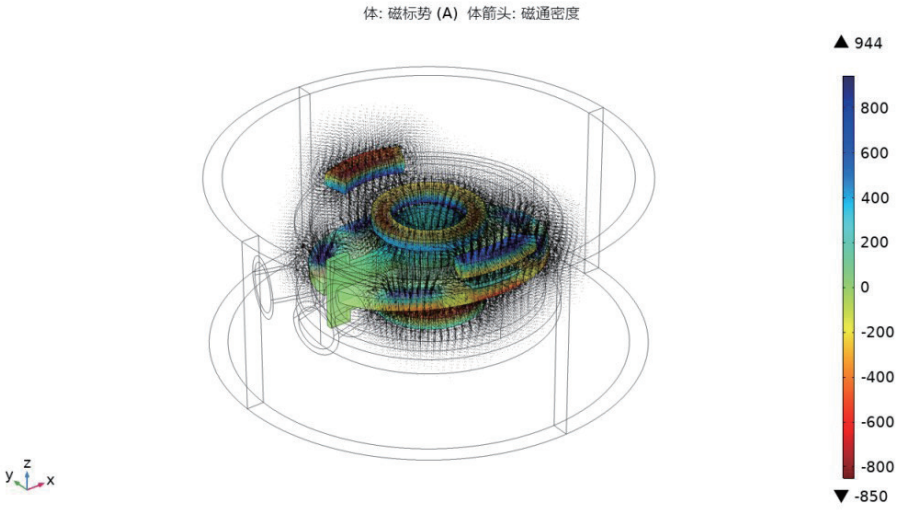

Fig. 5. (Color online) 3D magnetic density distribution around the pump rotor obtained using CFD.

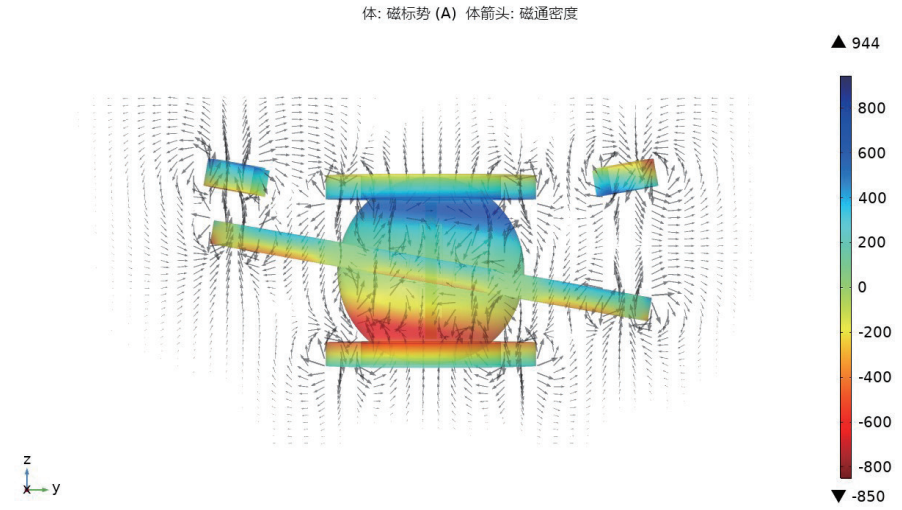

Fig. 6. (Color online) Magnetic density distribution (projected onto the *O-yz* plane) around the pump rotor obtained using CFD.

3.2 Effect of bearing permanent magnet size on levitated magnetic force

The levitation of the internal rotor of a blood pump bearing is achieved through the magnetic force generated in the biased permanent magnet rings. Therefore, the size of the permanent magnet rings is directly related to the levitated force magnitude and will impact the levitation stability of the rotor. In this section, keeping the size of the static magnetic ring of the bearing constant, we employed FEM to calculate changes in the magnetic force of the dynamic magnetic ring inside the rotor at different axial heights and radial thicknesses. The results are depicted in Figs. 7 and 8.

From the results shown in Figs. 7 and 8, it is evident that the magnetic force experienced by the blood pump rotor within one oscillation cycle is generally stable, with small changes of about 0.7 N for different ring heights and 0.4 N for different ring thicknesses. The comparison of the

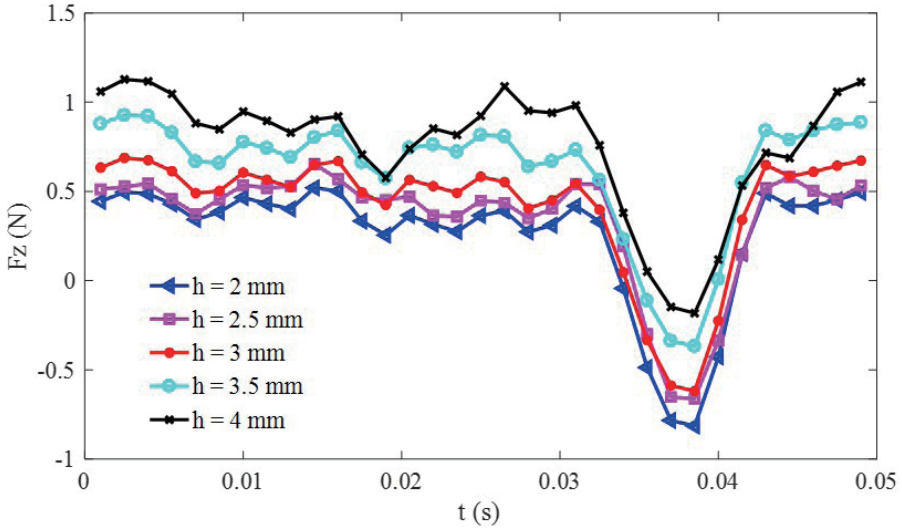

Fig. 7. (Color online) Variation of magnetic force with time at different heights of magnetic ring.

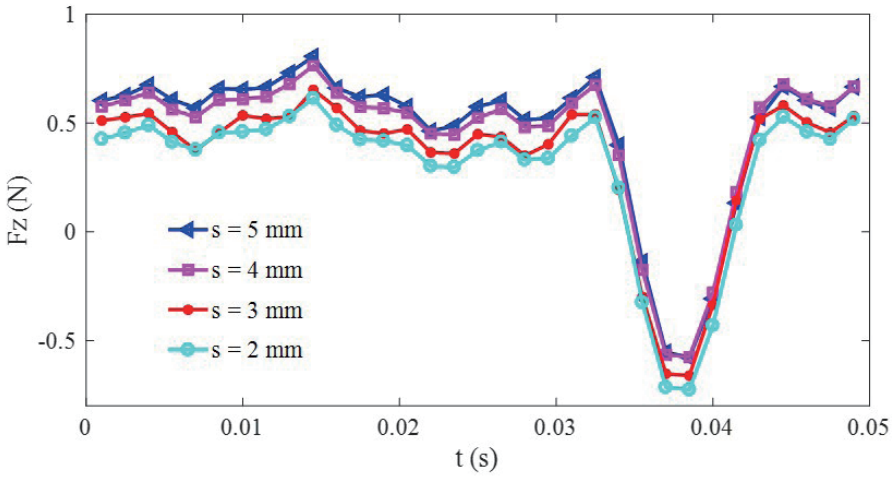

Fig. 8. (Color online) Variation of magnetic force with time at different radial thicknesses of magnetic ring.

effects of changes in ring height shows that the radial thickness has a minimal effect on the levitated magnetic force. Furthermore, note that the levitated magnetic force undergoes a sudden change at the moment of 0.0375 s for different ring heights and thicknesses, lasting approximately 0.0105 s, with a sudden change difference of approximately 0.93 N. This sudden change in levitated magnetic force is due to an opening in the swing disc of the suspended rotor, where it is not possible to install magnets. As the driving magnets rotate to this position, one end of the swing disc opening experiences zero magnetic force, while only the other end, symmetrically opposite to the opening, experiences levitated magnetic force. This leads to a sudden change in the levitated magnetic force of the rotor.

3.3 Effect of nutation angle on the levitated magnetic force and moment

The nutation angle is a crucial parameter that affects the optimal structure of a blood pump. With a constant radial size of the blood pump, a larger nutation angle corresponds to a greater axial space and a larger volume of the blood pump cavity. Additionally, the nutation angle is significant in determining the stability of the magnetically levitated blood pump. Given these considerations, we will later concentrate on studying the stability of the blood pump rotor at various nutation angles.

Under the same conditions of driving speed, magnetic suspension bearing size, and levitation gap as in Sect 3.2, we are currently investigating the variations of levitated magnetic force and moment over time for five different blood pump structures at various nutation angles. Since the proper axial size of the blood pump is directly related to the nutation angle, it is suggested that the nutation angles should all be within 10° on the basis of empirical considerations. Finally, through FEM calculations, we have obtained the variations of magnetic force and moment over time at different nutation angles, as shown in Figs. 9 and 10, respectively.

Figure 9 illustrates that when the nutation angle remains constant, the levitated magnetic force fluctuates over time between −0.8 and 0.6 N. There appears a local minimum of the

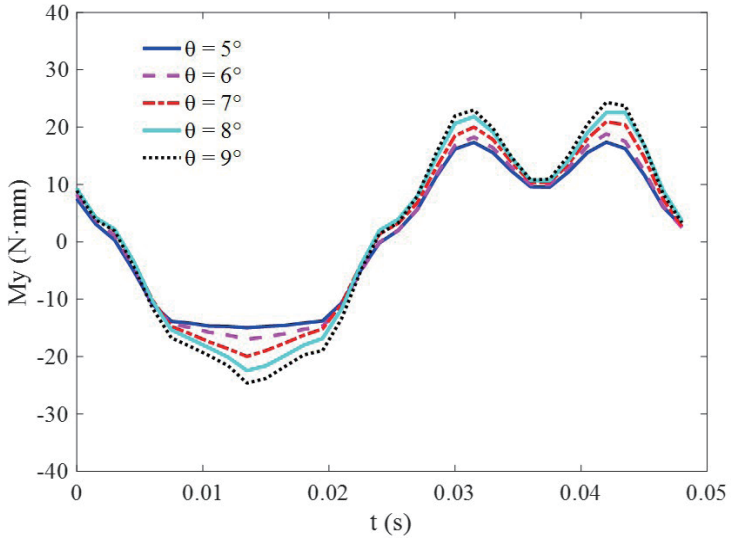

Fig. 9. (Color online) Variation of magnetic force with time at different nutation angles.

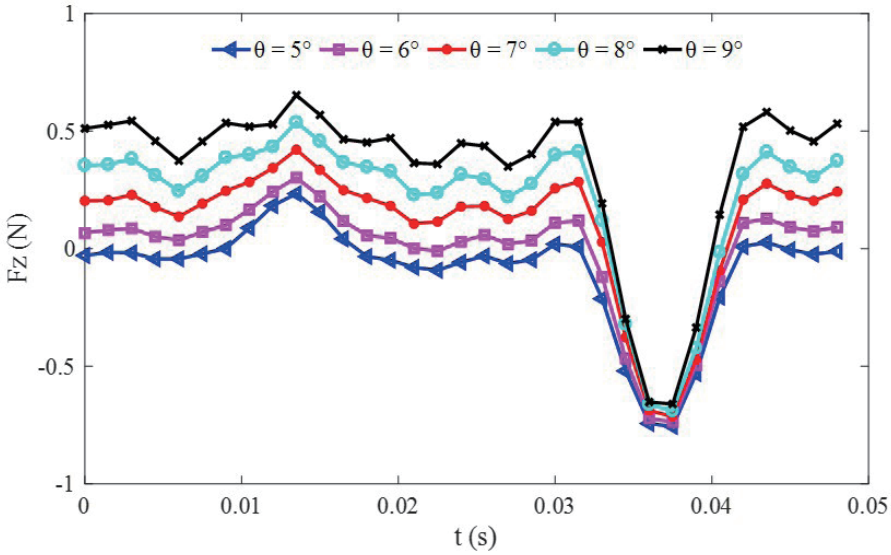

Fig. 10. (Color online) Variation of magnetic moment with time at different nutation angles.

levitated magnetic force occurring near $t = 0.0375$ s, corresponding to the position of the opening of the nutation disc. With the increase in nutation angle, the levitated magnetic force also increases. This is because as the nutation angle increases, the gap between the permanent magnet at the edge of the disc and the driving magnet decreases, resulting in an increase in driving magnetic force on the disc, and thus, the total levitation magnetic force of the rotor increases. Furthermore, as the nutation angle increases, the difference in the sudden change of the levitated magnetic force, where a local minimum occurs, also increases. This is because with a larger nutation angle, the driving magnetic force acting on the disc itself increases. Therefore, the difference in the sudden change of the magnetic force at the disc opening position is also larger.

Figure 10 indicates that the difference in magnetic moment is relatively small under various nutation angles. The greater the nutation angle, the higher the peak value of the magnetic moment. The magnetic moment of the rotor, overall, tends to decrease at approximately three-quarters of the time cycle and tends to increase for the remainder of the time cycle. The sudden drop in magnetic moment near $t = 0.014$ s is due to the fact that at this moment, the driving magnet rotates to the disc opening of the nutation. Since there is no magnet installed at the opening, the disc is subjected to an unbalanced force, with only one end of the magnet being driven. This imbalance leads to a steep drop in magnetic moment.

3.4 Effect of levitation gap on levitated magnetic force

Under the combined action of the external and internal permanent magnets of the bearing, the levitation gap significantly affects the dynamic stability of the blood pump rotor. To explore this effect, we conducted a study on four different blood pump structures at various levitation gaps. Through FEM calculations, we obtained the relationship between the levitated magnetic force of the blood pump rotor and time under different levitation gaps, and the results are shown in Fig. 11.

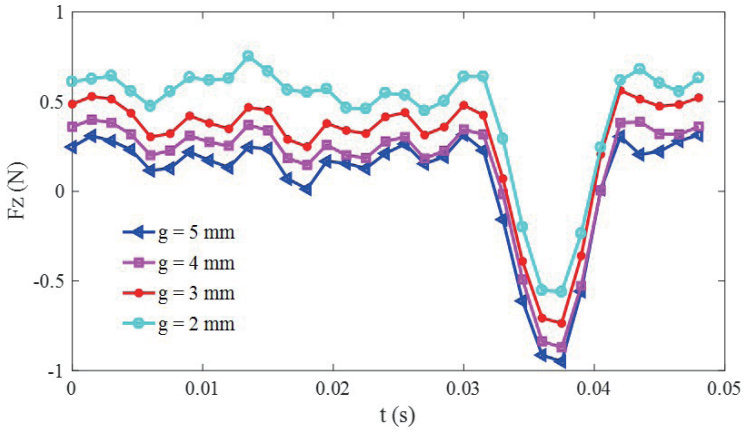

Fig. 11. (Color online) Variation of magnetic force with time at different levitation gaps.

Figure 11 shows that under the four different levitation gap conditions, the trend of levitated magnetic force over time is stable and consistent, with only a maximum change of about 0.6 N. The levitated magnetic force clearly increases as the levitation gap decreases. However, when the driving magnet rotates to the disc opening of the nutation, there is a sudden change in magnetic force similar to previous cases, but the difference in sudden change under different levitation gaps remains uncharged at approximately 0.925 N.

4. Experimental Measurement and Verification

To validate the FEM calculation results regarding the dynamic stability of the blood pump rotor, we constructed a hydraulic experimental system and conducted cyclic measurements on the blood pump. To simulate real blood flow, we used a 33% glycerol solution mixed with physiological saline as the test fluid, diluted to a viscosity similar to blood. Additionally, we established an experimental system for the real-time measurement and monitoring of the levitated state of the blood pump rotor, as shown in Fig. 12. This system integrates all types of required sensor: first, an electronic turbine flowmeter sensor connected to the outlet of the blood pump to measure the instantaneous output flow rate of the test fluid as the output flow rate of the blood pump; second, a pressure differential sensor to measure the pressure at the inlet and outlet of the blood pump; third, a photoelectric switch sensor to measure the speed of the blood pump; fourth, a noncontact eddy current sensor to measure the axial displacement of the rotor; fifth, force and moment sensors are used to measure the buoyancy and moment of the blood pump rotor, respectively.

The overall experiment is divided into two parts. The first part involves measuring the basic physical parameters of the blood pump, including the pressure difference, flow rate, and axial displacement. The measurement results can be used as input parameters for theoretical calculations. The second part involves measuring the magnetic force of the blood pump rotor, and the measurement results can be compared with the theoretical calculation results. The measurement results are shown in Table 1, which also includes the data obtained from previous FEM calculations. The table shows that the maximum error between the measured and FEM-

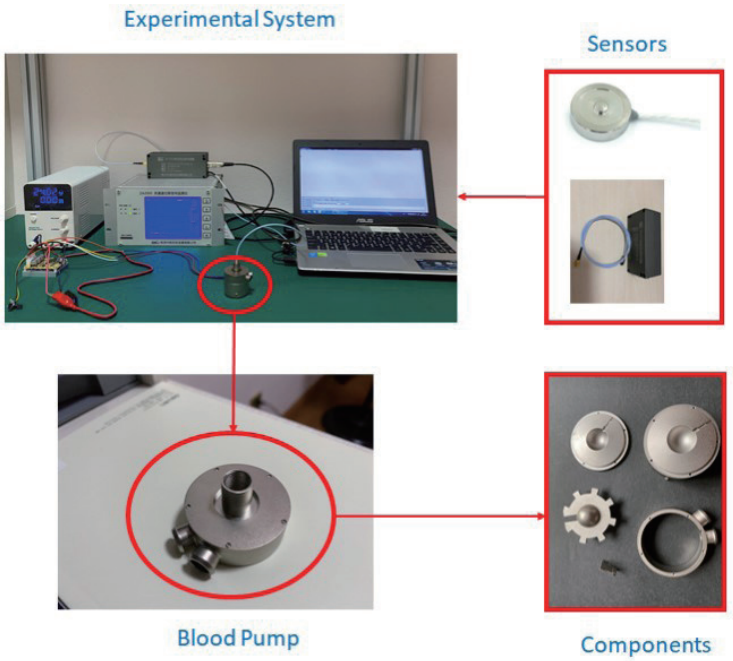

Fig. 12. (Color online) Sensor-based experimental setup.

Table 1
Measurement and calculation results of the magnetic force of the blood pump rotor at $s = 5$, $h = 3.5$, and $g = 2$ (1 cycle time: 0.05 s).

Magnetic force	$t = 0.01$ s	$t = 0.03$ s	$t = 0.04$ s	$t = 0.05$ s
Measurement (N)	0.636	0.63	−0.68	0.567
Calculation (N)	0.67	0.65	−0.74	0.6
Error (%)	5	7	8	5.5

obtained magnet forces is 8%. This comparison result indicates that the data obtained from the FEM calculations are sufficiently accurate, meaning that the results of the stability analysis of the blood pump rotor via FEM calculations are highly reliable and valuable.

5. Conclusion

We successfully established the Euler angle equation to describe the motion of the magnetically levitated rotor in a blood pump. Through FEM calculations, we thoroughly analyzed the factors affecting the dynamic levitation stability of the blood pump rotor. Moreover, we investigated the regularity and effects of three key factors, namely, the nutation angle, the height and thickness of the permanent magnet rings in the nutation blood pump bearing, and the levitation gap, on the levitation stability of the blood pump rotor. A significant finding is that the opening of the ring disc causes a sudden drop in levitated magnetic force as well as moment when the rotor is rotating. This could lead to a problematic situation when a blood pump is used for medical purposes. A comparative investigation shows that a maximum error of 8% was

found between the measured and calculated magnetic forces, indicating that the results of the stability analysis of the blood pump rotor via FEM calculations are highly reliable and valuable. The results of this study can further enhance our understanding of the blood pump's functionality and provide insights into the parameters affecting a well-designed blood pump.

Acknowledgments

This work was supported by the Special Project of the Central Government to Guide Local Scientific and Technological Development (Grant no. 2021L3046), the Project of the Department of Science and Technology of Fujian Province, China (Grant nos. 2021G02013, 2020H0049, and 2021H0060), and in part by the Sanming University of Fujian Province, China (Grant nos. 19YG05 and 19YG04).

References

1 G. Chen, L. G. Yao, K. C. Wang, J. X. Ding, and Z. Y. Wang: Sens. Mater. **33** (2021) 2665. https://doi.org/10.18494/SAM.2021.3395
2 G. Chen, L. Yao, R. Zheng, L. Zhang, and J. Ding: IEEE Access **7** (2019) 169327. https://doi.org/10.1109/ACCESS.2019.2955027
3 L. Wang, X. Tang, Z. Yun, and C. Xiang: Shock Vib. **2020** (2020). https://doi.org/10.1155/2020/8833994
4 P. Shen, Y. Wang, Y. Chen, P. Fu, L. Zhou, and Liu L: Machines **9** (2021) 255. https://doi.org/10.3390/machines9110255
5 G. Chen, L. G. Yao, K. C. Wang, J. X. Ding, and L. Wu: Sens. Mater. **34** (2022) 2199. https://doi.org/10.18494/SAM3821
6 S. Shida, T. Masuzawa, and M. Osa: Int. J. Artif. Organs **43** (2020) 774. https://doi.org/10.1177/0391398820917149
7 R. Kosaka, D. Sakota, M. Nishida, O. Maruyama, and T. Yamane: Int. J. Artif. Organs **24** (2021) 157. https://doi.org/10.1007/s10047-020-01240-6
8 N. Luo, S. Karnik, S. Kiang, P. A. Smith, N. Kurita, O. H. Frazier, and Y. Wang: 2022 23rd Int. Conf. the Computation of Electromagnetic Fields (COMPUMAG) (2022) 1–4. https://doi.org/10.1109/COMPUMAG55718.2022.9827510
9 T. Miyamoto, Y. Kado, A. R. Polakowski, D. J. Horvath, B. D. Kuban, K. Fukamachi, and J. H. Karimov: Int. J. Artif. Organs **44** (2020) 1055. https://doi.org/10.1111/aor.13690
10 W. Yang, S. Peng, W. Xiao, Y. Hu, H. Wu, and M. Li: Sensors **22** (2022) 1642. https://doi.org/10.3390/s22041642
11 P. Li, X. Mei, W. Ge, T. Wu, M. Zhong, N. Huan, Q. Jiang, P. L. Hsu, U. Steinseifer, N. Dong, and L. Zhang: Front. Physiol. **14** (2023). https://doi.org/10.3389/fphys.2023.1136545
12 P. Wu: Med. Novel Technol. Devices **16** (2022) 100177. https://doi.org/10.1016/j.medntd.2022.100177
13 S. Shida, T. Masuzawa, and M. Osa: Int. J. Artif. Organs **45** (2022) 52. https://doi.org/10.1177/0391398820984485
14 N. K. Ranganath, M. Rashidi, J. F. Antaki, K. G. Phillips, Z. N. Kon, D. E. Smith, A. Reyentovich, and N. Moazami: ASAIO J. **66** (2020) 343. https://doi.org/10.1097/MAT.0000000000000994
15 C. S. Fox, T. Palazzolo, M. Hirschhorn, R. M. Stevens, J. Rossano, S. W. Day, V. Tchantchaleishvili, and A. L. Throckmorton: Front. Cardiovasc. Med. **9** (2022). https://doi.org/10.3389/fcvm.2022.886874
16 Y. Li, Y. Xi, H. Wang, A. Sun, X. Deng, Z. Chen, and Y. Fan: Int. J. Numer. Methods Biomed. Eng. **39** (2022) e3671. https://doi.org/10.1002/cnm.3671
17 Z. Chen, S. K. Jena, and G. A. Giridharan: Int. J. Numer. Methods Biomed Eng. **34** (2018). https://doi.org/10.1002/cnm.2924
18 L. H. Tompkins, B. N. Gellman, and G. F. Morello: ASAIO J. **67** (2021) 1026. https://doi.org/10.1097/mat.0000000000001323
19 Y. Li, J. Yu, and H. Wang: Artif. Organs **46** (2022) 1817. https://doi.org/10.1111/aor.14265
20 P. Wu, J. Huo, W. Dai, W. T. Wu, C. Yin, and S. Li: Front Physiol. **12** (2021) 699891. https://doi.org/10.3389/fphys.2021.699891
21 C. H. Chan, I. L. Pieper, and R. Hambly: Artif. Organs **39** (2015) 93. https://doi.org/10.1111/aor.12351